ELSEVIER

Journal of Nuclear Materials 288 (2001) 187–196

journal of nuclear materials

www.elsevier.nl/locate/jnucmat

Studies on hydrogen permeability of 2.25% Cr–1% Mo ferritic steel: correlation with microstructure

N. Parvathavarthini, S. Saroja, R.K. Dayal *, H.S. Khatak

Materials Characterisation Group, Indira Gandhi Centre for Atomic Research, Kalpakkam 603102, India

Received 1 March 2000; accepted 18 October 2000

Abstract

The influence of microstructure on the hydrogen permeability, diffusivity and solubility in 2.25% Cr–1% Mo ferritic steel was investigated using electrochemical permeation technique. Varieties of microstructures ranging from martensite in water-quenched (WQ) steel to a predominant ferrite structure in annealed steel were characterised using analytical transmission electron microscopy. In the tempered structures, continuous precipitation of a variety of carbides of different morphologies and sizes was also characterised. The hydrogen diffusivity showed a continuous increase as the structure changed from martensite to ferrite and also with increasing extent of tempering. Solubility showed a corresponding decrease. The trends have been understood in terms of the number of reversible traps available for hydrogen in these different structures. Accordingly, martensite structure offered the maximum resistance to hydrogen diffusivity and tempered structure the least resistance due to the annihilation of defects during tempering and reduction in the solute content of the matrix due to precipitation.

1. Introduction

2.25% Cr–1% Mo ferritic steel is one of the most widely used and best characterised grade among the chrome–molybdenum steels. This alloy is generally used in steam generators where temperature may reach as high as 673–798 K. Pressure vessels and reactors used in the refining and processing of petroleum are commonly made of this steel. This alloy has gained worldwide acceptance by the nuclear industry and has been selected for the evaporator portions of the steam generator of liquid metal cooled fast breeder reactor [1] due to its acceptable mechanical properties up to 793 K and good fabricability and weldability [2–4]. The compatibility in sodium at the operating temperature of the steam generator [5], compatibility with normal and off-normal evaporator water and super-heated steam are the other important factors for the choice of this material in steam generator. This steel has been accepted for high-temperature service under section 3-ASME case 47 [6].

2.25% Cr–1% Mo ferritic steel is always used in the normalised and tempered condition or annealed condition. The carbides obtained during these heat treatments are of required morphology and distribution to impart the required strength to the steel by precipitation hardening. However, due to the metastable nature of the strengthening precipitates, they undergo undesirable transformation during elevated temperature service or during fabrication such as welding, forging and hot rolling. Occasionally thermal transients could cause excess local heating of the tubes, which can result in microstructural changes. All these situations would result in microstructural variations in the fabricated or service-exposed components quite different from the initial optimised microstructure obtained in normalised and tempered or annealed condition.

Operating experience with this ferritic steel indicates that this material is immune to chloride stress corrosion cracking in wetting steam conditions and reasonably resistant to localised corrosion [7]. However, exposure to very severe caustics in high concentrations or in combination with other impurities causes rapid failure of this steel. It has been reported that this steel is prone to hydrogen attack when exposed to high temperature

* Corresponding author. Fax: +91-4114 40 360.
E-mail address: rkd@igcar.ernet.in (R.K. Dayal).

0022-3115/01/$ - see front matter
PII: S0022-3115(00)00706-6

(over 523 K) and high-pressure hydrogen (over 2 MPa) [8,9]. Reaction between hydrogen and carbon in the steel results in the formation of methane bubbles which nucleate and grow preferentially along grain boundaries leading to loss of mechanical properties. However, during high-temperature service in a steam generator environment, where hydrogen fugacity is much less, hydrogen embrittlement is not a problem since atomic hydrogen can diffuse out rapidly in BCC/BCT structure at elevated temperatures. However, when this steel is exposed to ambient conditions during fabrication, storage, inspection or commissioning, the material undergoes general corrosion and corrosion-generated hydrogen can penetrate into this material which can result in hydrogen-induced cracking (HIC) [10]. During fusion welding (either during fabrication or repair welding), atomic hydrogen is absorbed in the steel. This can rapidly diffuse to the heat-affected zone at ambient temperature and can result in cold cracking even before post-weld heat treatment is performed. Therefore this material is highly susceptible to HIC under ambient conditions.

It is well known that for HIC to initiate and propagate, hydrogen has to be transported within the material which depends upon the permeability of the material. Crack growth rate is also controlled by the rate of supply and accumulation of hydrogen at crack tip. Permeability depends upon the microstructure and it has been reported that as-quenched martensite has the lowest diffusivity as compared to other microstructures such as bainite or ferrite/pearlite [11–15]. It has been found that martensite occludes the maximum hydrogen compared to all other microstructures [16]. Sakamoto and Mantani have reported that D_{app} (apparent diffusivity in the presence of traps) increases with increase in temperature and solubility decreases with increase in degree of tempering [17,18]. A contrasting view has been reported by other groups [19,20]. Gerberich [21] had determined the D_{app} for a variety of steels and had reported one-to-one correlation with crack growth rate. A lot of literature is available on the influence of microstructure on hydrogen permeability, diffusivity and solubility in carbon steel but little work has been published on alloy steel.

The aim of the present investigation is to understand the influence of microstructure on hydrogen permeability. Hydrogen permeation measurements were carried out using Devanathan's technique. Detailed analytical electron microscopy was carried out to characterise the microstructure obtained during (i) solutionising and cooling at different rates, and (ii) normalising and tempering of 2.25% Cr–1% Mo ferritic steel in order to correlate the variations in microstructure with hydrogen permeability, diffusivity and solubility.

Table 1
Chemical composition of 2.25% Cr–1% Mo ferritic steel

Element	Weight (%)
Carbon	0.11
Silicon	0.31
Manganese	0.5
Phosphorous	0.025
Chromium	2.25
Molybdenum	0.9
Iron	Balance

2. Experimental procedure

The material used in this investigation was nuclear grade 2.25% Cr–1% Mo ferritic steel supplied by M/S Visvesaraya Iron and Steel Works, Badravathi in the hot-rolled condition. The chemical composition is given in Table 1. Circular specimens (diameter 25 mm and thickness 1.5 mm) were cut for permeation studies. The specimens were sealed in a quartz tube, evacuated to 10^{-4} Torr and subjected to various heat treatments to obtain different microstructures. The details of the heat treatments are given in Tables 2 and 3. Since several heat-treatment routes were adopted, each route is assigned a suitable designation which will be followed throughout the text.

The analytical transmission electron microscopy studies on carbon extraction replicas of the heat treated 2.25% Cr–1% Mo ferritic steel was carried out using a Philips CM 200 ATEM with an EDAX analyser with super-ultra-thin window at an operating voltage of 120 kV and spot size of 50–100 nm. The details of the analysis procedure are given elsewhere [22,23]. The Cu K_α peak (8.04 keV) in the EDAX spectrum arises due to the Cu grids used to prepare the carbon extraction replicas. For the purpose of quantification of the EDAX

Table 2
Details of the heat treatments and hardness during cooling of austenite[a]

Designation	Heat treatment	Macrohardness (VHN) (load – 10 kg)	Microhardness (VHN)
WQ	1193 K–1 h–WQ	372	–
AC	1193 K–1 h–AC	295	–
FC	1193 K–1 h–FC	135	(Ferrite) – 152 (Bainite) – 225

[a] WQ – water-quenching; AC – air-cooling; FC – furnace-cooling.

Table 3
Details of the heat treatments and hardness during tempering of normalised steel

Designation	Heat treatment	Macrohardness(VHN) (load – 10 kg)
AC	1193 K–1 h–AC	295
AC1a	1193 K–1 h–AC + 973 K–1 h–AC	214
AC8a	1193 K–1 h–AC + 973 K–8 h–AC	193
AC1b	1193 K–1 h–AC + 1023 K–1 h–AC	173
AC8b	1193 K–1 h–AC + 1023 K–8 h–AC	154

spectra (Tables 4 and 5), the Cu K_α peak has been ignored.

The permeation experiments were carried out using a specially designed experimental setup and the details of the specimen holder assembly and electrochemical double cell are given in our earlier publication [24]. The circular specimens for which hydrogen permeability is to be investigated was polished up to 600 grit using silicon carbide paper on one side and was electroplated with palladium on the other side. The details of the plating procedure adopted are also given in our earlier publication. Then the specimen was assembled in the specimen holder assembly. The permeation cells were firmly attached to the holder assembly in such a way that the palladium-coated surface faces the anodic compartment and the as-polished surface, the cathodic compartment from where hydrogen was generated. The anodic compartment was filled with 0.1 M NaOH solution and oxygen-free, dry argon gas was purged for 1 h. Then −40 mV (SCE) was applied to the specimen and the anodic current was recorded using a strip chart recorder. Within 1 h, the anodic current became stabilised. The background current was recorded. Then the cathodic compartment was filled with 0.5 M H_2SO_4 solution containing 200 ppm As_2O_3. In this compartment also, argon gas was purged. Using potentiostat in galvanostatic mode, cathodic current of 0.05 mA/cm^2 was applied. Hydrogen permeated through the specimens to the anodic side where it was instantaneously oxidised and turned into an equivalent current. Therefore, the permeation current density (P_t) at the exit side is a direct measure of the output flux of hydrogen. The variation in P_t with respect to time was monitored until steady state is reached. The rate of hydrogen permeation rises after certain breakthrough time (t_b) and then approaches asymptotically to the steady-state permeation current density (P_∞).

Table 4
Microchemical details of carbides formed during cooling of austenite

Designation	Type of carbides	% element in metal sublattice		
		Mo	Cr	Fe
AC	M_3C	7.26	1.41	91.33
FC	M_2C	25.47	63.01	11.52
	M_3C	10.80	29.16	60.04

Table 5
Microchemical details of carbides formed during tempering

Designation	Type of carbides	% element in metal sublattice		
		Mo	Cr	Fe
AC	M_3C	7.26	1.41	91.33
AC1a	M_3C	9.08	22.87	68.05
	M_2C	35.83	56.5	7.67
	M_7C_3	5.8	54.18	40.02
AC8a	M_2C	41.23	56.36	2.41
	M_7C_3	4.51	58.97	36.52
	$M_{23}C_6$	3.46	26.35	70.19
AC1b	M_2C	38.04	35.3	26.66
	M_7C_3	5.29	52.11	42.6
	$M_{23}C_6$	6.79	32.6	60.61
AC8b	$M_{23}C_6$	3.83	55.1	41.07
	M_6C	75.78	21.88	2.34

From P_∞, permeability (p) was calculated using the expression, $p = P_\infty/ZF$ where Z is the number of electrons participating in the reaction and F is Faraday's constant. Each experiment was repeated four times for all the heat-treated specimens. From breakthrough time (t_b), D_{app} was calculated using the expression, $D_{app} = L^2/15.3t_b$. From p and D_{app}, solubility (S) was calculated using the expression, $p = D_{app}S$.

3. Results and discussion

3.1. Microstructural variations in 2.25% Cr–1% Mo ferritic steel

3.1.1. Transformation of austenite in 2.25% Cr–1% Mo ferritic steel during cooling

In the present study, a wide range of cooling rates have been employed ranging from ~6000 K/min during water-quenching (WQ), ~120 K/min during air-cooling (AC) and ~2 K/min during furnace-cooling (FC) [25]. It is expected that such a marked variation in the cooling

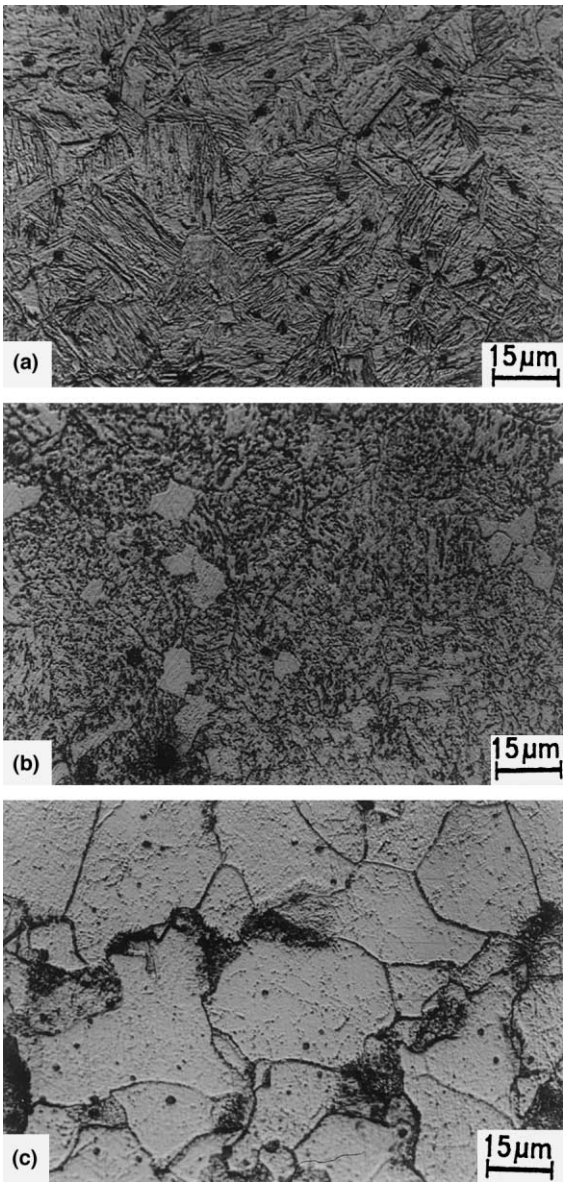

Fig. 1. Optical micrographs showing the room temperature microstructure of 2.25% Cr–1% Mo steel austenitised at 1193 K and cooled at various rates. (a) Fully martensitic structure in WQ. (b) Bainitic structure in AC. (c) Mixture of proeutectoid ferrite and bainite in FC.

rates would yield a wide variety of microstructures in this steel.

Figs. 1(a)–(c) show the optical micrographs of the 2.25% Cr–1% Mo ferritic steel cooled at different rates by various procedures. A completely martensitic structure is seen in WQ steel (Fig. 1(a)), while a bainitic structure is obtained in the normalised (AC) steel (Fig. 1(b)). The hardness of the steel decreases from 372 to 295 VHN as the cooling rate is reduced. Very slow cooling in the furnace produces a microstructure consisting of proeutectoid ferrite and small amounts of granular bainite (Fig. 1(c)). The formation of polygonal proeutectoid ferrite during FC can be confirmed from the microhardness values in the ferrite and bainite phases which are 152 and 225 VHN, respectively. The above microstructures are in agreement with the microstructures expected from the CCT diagram for 2.25% Cr–1% Mo ferritic steel for similar rates of cooling [26].

Detailed ATEM studies on carbon extraction replicas of the AC and FC specimens were carried out. Figs. 2(a)–(d) show the micrographs and EDAX spectra taken from representative precipitates. It can be seen that AC specimen (Fig. 2(a)) shows the presence of a few lenticular precipitates. The EDAX spectrum (Fig. 2(b)) shows that these carbides are Fe-rich, M_3C type of carbides. The FC specimen consists of predominantly ferrite and needle-like carbides (Fig. 2(c)). The inset in Fig. 2(c) shows a SAD pattern taken from one of the needle-like precipitates which has been identified as $\langle 1\,0\,\bar{1}\,0\rangle$ M_2C. The EDAX spectrum (Fig. 2(d)) from this needle-like precipitate showed that it is rich in Mo, though it also contains appreciable amounts of Cr. In addition to M_2C, the presence of coarse Fe-rich M_3C carbides has also been observed in the FC specimens. These microstructures are in complete agreement with other studies in this steel [27].

3.1.2. Tempering behaviour of 2.25% Cr–1% Mo ferritic steel

The normalised (AC) 2.25% Cr–1% Mo ferritic steel was tempered at 973 and 1023 K for various durations. The resultant microstructures are shown in Figs. 3 and 4. Table 3 lists the variation in hardness of the steel. The decrease in hardness with increase in tempering temperature and time at the two tempering temperatures can be understood in terms of the substructure changes associated with the dissolution of bainite, formation of ferrite and carbides. Additionally, the continuous precipitation of different carbides and coarsening of precipitates brings about a reduction in the solute content (mainly C and Mo) and hence the hardness. The consistently lower values at 1023 K for the same duration can be understood in terms of the faster kinetics at 1023 K.

Detailed TEM analysis on carbon extraction replicas of the tempered specimens was carried out to identify the type and composition of the carbides which are listed in Tables 4 and 5. On tempering, the bainite in AC specimens with lenticular, aligned M_3C undergoes several changes like formation of proeutectoid ferrite, nucleation of secondary carbides and growth of precipitates. Tempering at 973 K for 1 h resulted in dissolution of bainite and formation of a large number of precipitates, predominantly on grain boundaries (Fig. 3(a)). These precipitates have been identified by selected area diffraction (shown as insets in Fig. 3(a)) as

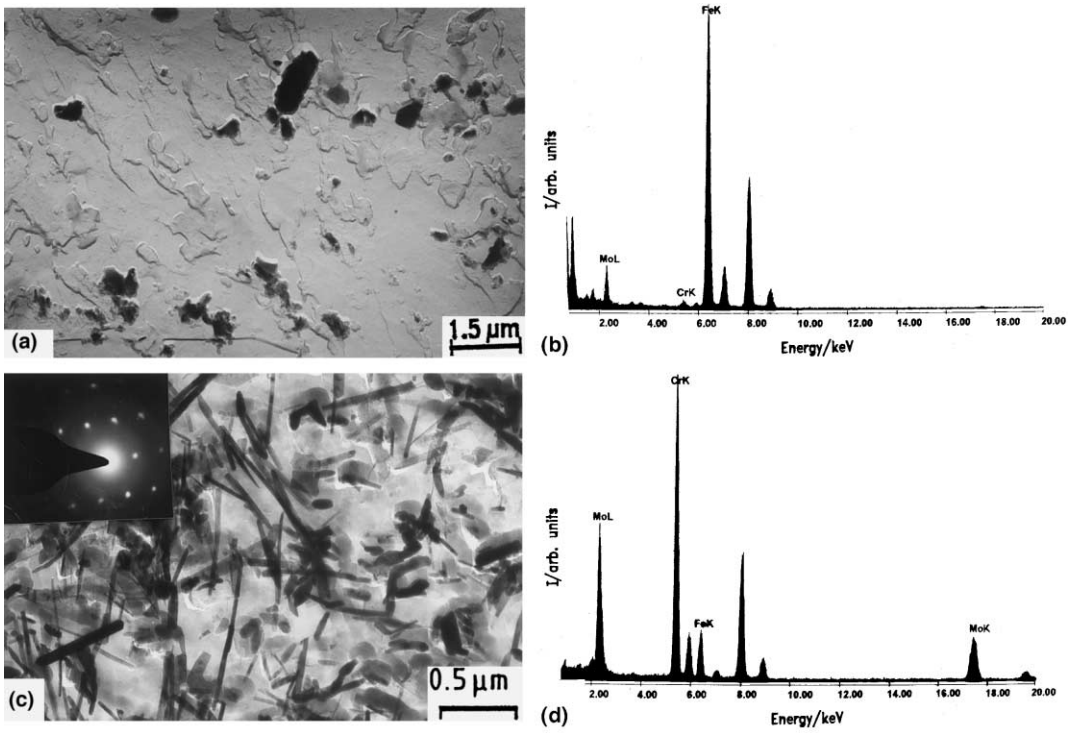

Fig. 2. TEM micrograph of the carbon extraction replica of 2.25% Cr–1% Mo steel austenitised at 1193 K. (a) Presence of lenticular carbides in AC specimen. (b) EDAX spectrum from one of the carbides showing that it is of Fe-rich M_3C type. (c) Presence of fine needle-like carbides within ferrite in FC specimen. Inset shows the SAD pattern from one of these carbides confirming the presence of $\langle 10\bar{1}0\rangle$ M_2C. (d) EDAX spectrum from the needle-like carbide in ferrite showing the enrichment of Mo and Cr in M_2C.

M_3C and M_7C_3. The EDAX spectrum from these precipitates are shown in Figs. 3(b) and (c). M_3C precipitates are especially Fe-rich, but also accommodate significant amounts of Cr and Mo while the M_7C_3 precipitates are Cr-rich with Fe and Mo. The fine intralath carbides were found to be rich in Mo, belonging to M_2C type (Fig. 3(d)). Further tempering for 8 h resulted in the coarsening of precipitates (Fig. 3(e)). The coarse globular and lenticular carbides on grain boundaries have been identified as $M_{23}C_6$ (selected area diffraction pattern shown as an inset in Fig. 3(e)). The EDAX spectrum from a typical $M_{23}C_6$ precipitate (Fig. 3(f)) shows that they are Fe-rich, but also contain large amounts of Cr. In addition to $M_{23}C_6$, a few rod-like Cr-rich M_7C_3 (SAD pattern given as inset in Fig. 3(e)) and Mo-rich M_2C were also observed within the grains. The variation in the solute content with tempering temperature and time in each type of carbide can be clearly seen from Table 5.

Tempering at 1023 K for 1 h produced considerable reduction in hardness. The microstructure (Fig. 4(a)) consists of ferrite structure with a fine distribution of carbides on lath and grain boundaries. They have been identified by diffraction (inset in Fig. 4(a)) as $M_{23}C_6$. In addition to $M_{23}C_6$, Cr-rich M_7C_3 and M_2C were also present within the grains. Further tempering for 8 h resulted in the formation of only coarse $M_{23}C_6$ carbides of different morphologies at boundaries (Fig. 4(b)). The diffraction pattern from a boundary carbide shown as an inset in Fig. 4(b) confirms that this carbide is of $M_{23}C_6$ type. The EDAX spectrum from this $M_{23}C_6$ carbide is shown in Fig. 4(c). It can be seen that the Cr content of this carbide is very high when compared to the $M_{23}C_6$ carbides at lower tempering temperatures which had very high amounts of iron (Table 5). The high Cr content at 1023 K after tempering for 8 h is attributed to the higher diffusivity of Cr at higher temperatures and the stability of Cr-rich $M_{23}C_6$ carbides. In addition to M_6C, M_7C_3 and $M_{23}C_6$, nucleation of a few Mo-rich precipitates were also seen. The diffraction pattern from the arrow marked carbide (inset in Fig. 4(b)) suggests the presence of M_6C carbides. The EDAX spectrum (Fig. 4(d)) from the arrow marked M_6C shows that though they are rich in Mo, they contain appreciable amounts of Cr and small amounts of Fe. The M_6C carbides are microchemically similar to the M_2C carbides suggesting early stages of precipitation of the M_6C.

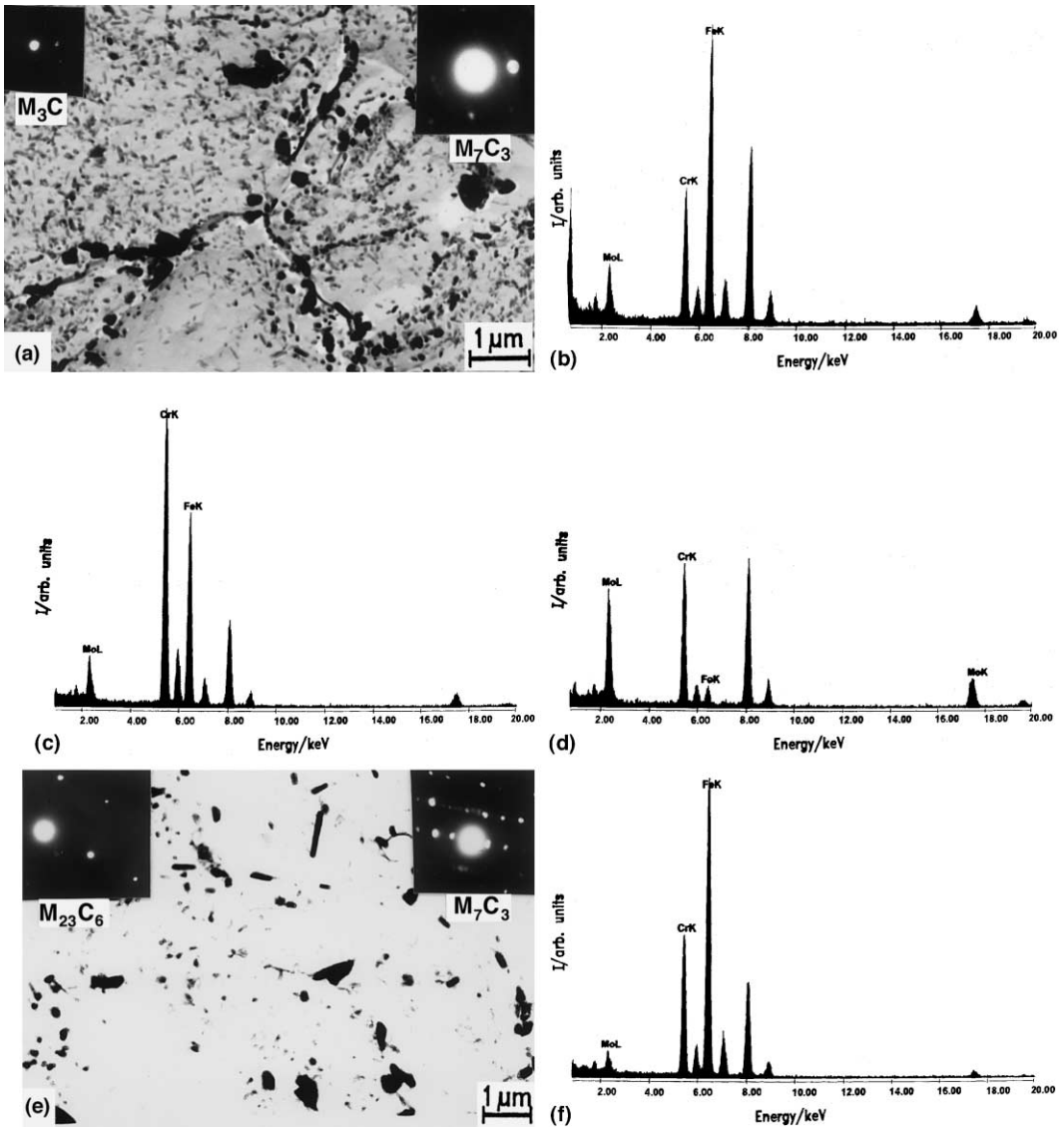

Fig. 3. TEM micrograph of the carbon extraction replica of normalised and tempered 2.25% Cr–1% Mo steel (AC1a) showing the presence of intra and interlath precipitates. (a) Tempering at 973 K for 1 h results in the formation of fine acicular intralath carbides and coarse boundary carbides. Inset shows the SAD pattern of $\langle 1\bar{7}2\rangle$ M_3C and $\langle 2\bar{3}0\rangle$ M_7C_3. (b) EDAX spectrum from boundary carbide showing that the M_3C carbides are Fe-rich. (c) EDAX spectrum from a rod-like M_7C_3 showing the enrichment of Cr. (d) EDAX spectrum from the fine, needle-like M_2C showing the enrichment of Mo TEM micrograph of the carbon extraction replica of normalised and tempered 2.25% Cr–1% Mo steel (AC8a). (e) Coarsening of the carbides after tempering for 8 h at 973 K. Insets show the SAD pattern from a boundary carbide confirming the presence of $\langle 100\rangle$ $M_{23}C_6$ and from a rod-like intragranular carbide confirming the presence of $\langle 1\bar{4}1\rangle$ M_7C_3 along the boundaries. (f) EDAX spectrum from $M_{23}C_6$ carbide show that it is Fe-rich with large amounts of Cr.

3.2. Electrochemical permeation studies

3.2.1. Hydrogen permeation behaviour in quenched, normalised and annealed steel

The permeability (p) and D_{app} obtained from permeation transients and solubility calculated from p and D_{app} for all the heat-treated specimens are collectively presented in Tables 6 and 7. It has been reported that the diffusivity of hydrogen in pure α-iron is very high and is of the order of 10^{-5} cm^2/s [28] and diffusivity in low-alloy ferritic steel is about the same as that of α-iron. However, in this steel the diffusivity is lower by two orders of magnitude for WQ and AC material, whereas for normalised and tempered or annealed material, it is

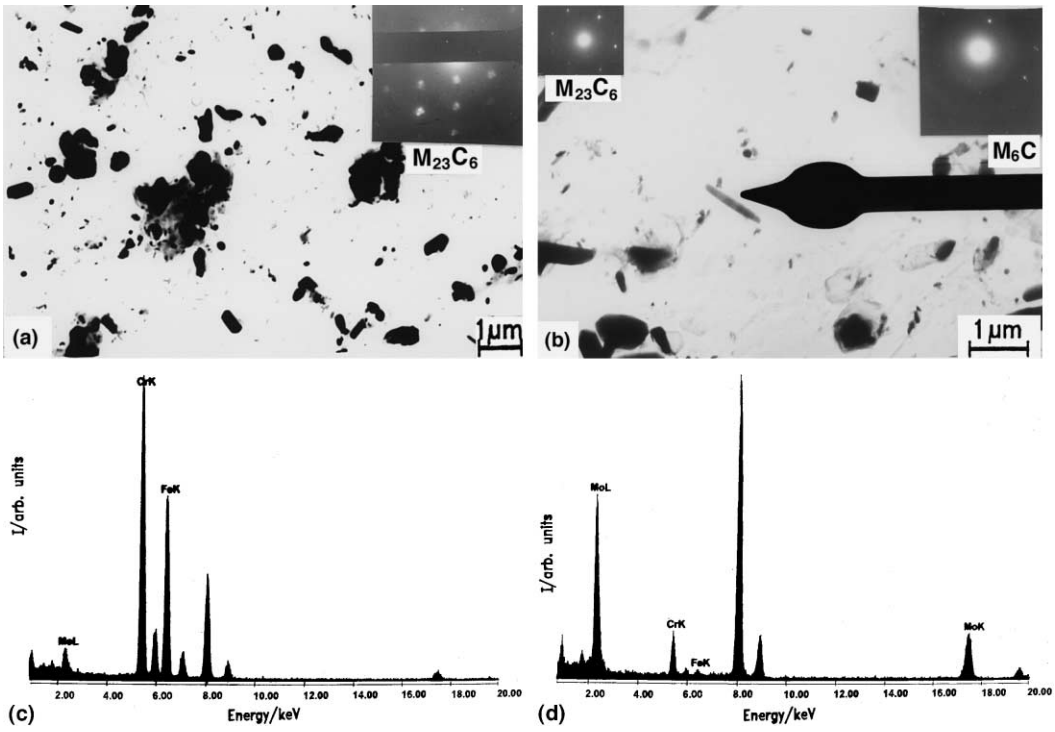

Fig. 4. TEM micrograph of the carbon extraction replica of normalised and tempered 2.25% Cr–1% Mo steel. (a) Tempering at 1023 K for 1 h results in ferrite structure with carbides distributed on lath and grain boundaries. Inset shows the SAD pattern from a boundary carbide identified as $\langle 1\,\bar{2}\,1\rangle$ $M_{23}C_6$. (b) Coarsening of carbides after 8 h of tempering. Insets show the SAD patterns from the two types of carbides identified as $\langle 1\,\bar{1}\,1\rangle$ $M_{23}C_6$ and $\langle 2\,\bar{1}\,0\rangle$ M_6C (arrow marked carbide). (c) EDAX spectrum from $M_{23}C_6$ showing higher levels of Cr in contrast to the Fe-rich $M_{23}C_6$ at lower temperature. (d) Enrichment of Mo in the arrow marked M_6C carbide is seen though it also contains significant amount of Cr.

Table 6
Permeability (p), diffusivity (D) and solubility (S) of hydrogen during cooling of austenite in 2.25% Cr–1% Mo ferritic steel

Heat treatment	$p \times 10^{12}$ mol/cm s	$D \times 10^{7}$ cm^2/s	$S \times 10^{5}$ mol/cm^3
WQ	6.80 ± 0.35	4.47 ± 0.24	1.52 ± 0.06
AC	7.75 ± 0.12	5.19 ± 0.39	1.49 ± 0.09
FC	9.44 ± 0.38	40.00 ± 2.98	0.24 ± 0.01

Table 7
Permeability (p), diffusivity (D) and solubility (S) of hydrogen during normalising and tempering in 2.25% Cr–1% Mo ferritic steel

Heat treatment	$p \times 10^{12}$ mol/cm s	$D \times 10^{7}$ cm^2/s	$S \times 10^{5}$ mol/cm^3
AC	7.75 ± 0.12	5.19 ± 0.39	1.49 ± 0.09
AC1a	8.04 ± 0.18	9.82 ± 0.67	0.83 ± 0.07
AC8a	8.31 ± 0.08	12.00 ± 0.18	0.69 ± 0.01
AC1b	6.86 ± 0.15	16.00 ± 0.18	0.43 ± 0.01
AC8b	6.83 ± 0.06	32.70 ± 1.87	0.21 ± 0.01

an order of magnitude lower. This is due to the presence of lattice defects such as grain boundaries, dislocations or precipitate/matrix interfaces which are favourable sites for trapping of hydrogen.

The WQ material which has lath-martensitic structure shows the highest solubility and lowest diffusivity compared to all other microstructures of 2.25% Cr–1% Mo steel. The martensitic structure has very high dislocation density, which acts as efficient reversible traps for hydrogen [29,30]. Additionally, the lath structure in martensite which contributes to a large grain boundary area also provides a large number of trap sites. These

arise due to the carbon atoms retained in the α-iron lattice during fast quenching which introduce a high degree of lattice strain in the martensite matrix. Autoradiographic studies have confirmed that hydrogen gets trapped at dislocations, point defects, subgrain boundaries, voids, lath-boundaries and precipitate/matrix interfaces [31,32]. Generally hydrogen traps are classified as reversible or irreversible according to their binding energy. Traps are considered irreversible if the trapped hydrogen is not relaxed at room or at low temperatures. A further classification of the different trap sites based on the binding energy of the trap with hydrogen in α-Fe lattice shows essentially three classes of traps [31]:

1. Very weak traps: Dislocations (binding energy ~20 kJ/mol) and fine precipitates in the matrix are classified in this category. It may be appropriate to include solutes like Cr and Mo also whose binding energies are reported to be around half of that of dislocations [33].
2. Intermediate traps: Martensite laths and prior austenite grain boundaries (binding energy ~50 kJ/mol) [34] fall in this category.
3. Strong traps: These traps gets degassed only at high temperatures. Non-metallic inclusions, spherical precipitates, interfaces of martensite laths and/or prior austenite grain boundaries with retained austenite, fine precipitates or impurity segregations are included in this class (binding energy ~100–120 kJ/mol).

The observed diffusivity in the WQ samples which is the lowest can be clearly understood from the above discussion. The D_{app} reported for martensite in this steel is lower than that for martensite in plain carbon steel. Valentini and Solina [31] have also observed the same trend and they have attributed this to the presence of solute atoms such as Mo and Cr which also act as weak traps for hydrogen. In particular, Cr concentrations of the same order of magnitude as those studied in the present study can reduce diffusivity by one order of magnitude. Our earlier studies with 9% Cr–1% Mo ferritic steel [24] indicate that when Cr level increases to 9% by weight, the D_{app} of martensite is of the order of 10^{-8} cm^2/s (two orders of magnitude less than that of martensite in plain carbon steel) which strongly supports the fact that Cr and Mo also act as weak trap sites for hydrogen.

The microstructure of normalised (AC) steel consists of bainite with fine acicular M_3C. From Table 6 it can be seen that the solubility of hydrogen in bainite is almost same (or marginally less) as that of martensite and D_{app} is marginally higher. It must be mentioned here that this electrochemical technique is very sensitive, so even minor variations in D_{app} and solubility can be measured. The lower cooling rate encountered during AC compared to that of WQ results in the reduction in defect density in bainite. The bainitic laths are also comparatively coarser than the matensitic laths. This is clearly indicated by the lower hardness value of bainite (295 VHN) compared to that of martensite (372 VHN) (Table 2,3). Therefore the contribution to hydrogen trapping associated with defects and grain boundaries is reduced resulting in an increase in diffusivity. However, this increase is partly compensated by the M_3C interfaces which also could act as trap sites (binding energy ~80 kJ/mol) [34]. Hence only a slight overall increase in diffusivity is seen between martensite and bainite structures.

The significant decrease in solubility and increase in D_{app} in the annealed material is consistent with its microstructure consisting of a high fraction of proeutectoid ferrite and granular bainite with randomly distributed cementite and needle-shaped M_2C in ferrite. From Table 6 it is seen that solubility is an order of magnitude lower and D_{app}, an order of magnitude higher than martensite and bainite. These observations can be rationalised as follows:

(i) Reduction in defect density and substructure changes due to decrease in cooling rate leads to a reduction in the number of trap sites.

(ii) The solute atoms such as Cr and Mo which also act as trap sites (when present in solid solution) participate in precipitation reactions and hence their contribution to trapping is also reduced.

(iii) The role of precipitates in acting as reversible trap sites is limited which was also observed in our earlier work on 9% Cr–1% Mo steel. The drastic reduction of defect density and grain boundary area due to the formation of proeutectoid ferrite product during annealing (FC) far outweighs the contribution from precipitates which will be discussed in detail in the next section.

Due to the above factors trapping and hence the solubility of hydrogen is very less and D_{app} is the highest for annealed (FC) material compared to all other microstructures in 2.25% Cr–1% Mo steel.

3.2.2. Hydrogen permeation behaviour in tempered steel

Tempering of the normalised steel leads to the dissolution of bainitic ferrite and cementite, precipitation of a number of metastable carbides and to the onset of recovery and recrystallisation process to different extents depending on the tempering temperature and time. The tempered steel can be classified in the order of AC1a, AC8a, AC1b and AC8b with increasing degree of tempering based on the hardness values which progressively decrease in the above order. It is well known that as the degree of tempering increases, the extent of annihilation of lattice defects increases. In the very initial stages, when the M_2C precipitates are coherent or semi-coherent with the matrix, the residual microstrain associated with them makes their interfaces traps for hydrogen [33]. As the degree of tempering increases, the dissolution of bainite laths to polygonal ferrite, dissolution of fine

M_3C and M_2C type of precipitates and precipitation of coarse M_7C_3 and $M_{23}C_6$ type of precipitates reduces the number of reversible hydrogen trap sites considerably. This is directly reflected in the continuously decreasing solubility and increasing value of D_{app}. It is reported that M_7C_3 and $M_{23}C_6$ type of carbides act as irreversible traps [33]. Additionally, the locking up of Mo by the M_2C precipitates and even M_6C at higher temperature causes a depletion of Mo in the lattice which again reduces the number of trapping sites, and hence increases diffusivity.

The influence of coherent precipitates in their initial stages of precipitation which would have acted as efficient traps [33] has not been studied in this investigation.The permeation behaviour after tempering for the duration of 1 and 8 h at 973 and 1023 K has been studied during which the role of precipitates as reversible hydrogen trap sites has become limited due to their nature and coarse size. Under these conditions, it can be seen that decrease in trap sites with increasing degree of tempering can be attributed to a combination of the following factors:

(i) annihilation of lattice defects and formation of polygonal ferrite associated with the dissolution of bainite;
(ii) decrease in solute atoms like Cr and Mo due to their involvement in precipitation;
(iii) formation of relatively coarse carbides, hence their interfaces do not act as reversible traps.

The salient features of this investigation are as follows:

(i) microstructural features which impart strain to the lattice such as defects, lath structure, solutes in solid solution and precipitates exert a strong influence on the hydrogen permeability in 2.25% Cr–1% Mo steel.
(ii) Lattice defects, lath boundaries and coherent precipitates act as strong trap sites for hydrogen. The observed values of diffusivity, solubility and hydrogen permeability is the result of the interplay of the above mentioned factors which contribute to the number of reversible traps.

4. Summary

The influence of microstructure on the hydrogen permeability, diffusivity and solubility in 2.25% Cr–1% Mo steel has been studied using Devanathan's electrochemical technique. It has been established in this study that lattice defects act as most effective traps for hydrogen. The martensitic structure obtained in WQ 2.25% Cr–1% Mo steel offered the maximum resistance to hydrogen permeation. The permeation experiments indicate that D_{app} shows an ascending trend with increasing degree of tempering due to annihilation of lattice imperfections, reduction in grain boundary area and reduction in solute Cr and Mo content (which are trap sites) during tempering. These effects have a more dominant role in influencing hydrogen permeability than the precipitates.

Acknowledgements

The authors acknowledge the support of Dr Baldev Raj, Director of the Materials, Chemistry and Reprocessing Group and Dr V.S. Raghunathan, Associate Director, Materials Characterisation Group, Kalpakkam during the course of this investigation. The authors are thankful to Dr Shaju K. Albert for the useful discussions during the course of this investigation. The authors thank Smt.K. Parimala for her assistance in the permeation experiments.

References

[1] L.M. Wyatt, in: S.A.Pugh, E.A.Little (Eds.), Proceedings of the BNES International Conference on Ferritic Steels for Fast Reactor Steam Generators, London, 1978, p. 27.
[2] G.N. Emmanuel, W.E. Leyda, E.J. Rozic, in: Symposium on 2.25% Cr–1% Mo Steel in Pressure Vessel and Piping, ASME-MPC, Denver, CO, 1970.
[3] R.H. Zeisloft, W.E. Leyda, H.A. Domain, in: Low carbon and stabilized 2.25 Cr–1 Mo steels, ASM, 1970.
[4] R.L. Klueh, J. Nucl. Mater. 54 (1974) 55.
[5] T. Wada, G.T. Eldis, in: Ashok K. Khare (Ed.), Application of 2.25 Cr–1 Mo steel for Thick Wall Pressure Vessels, ASTM STP 755, ASTM, 1982, p. 343.
[6] D. Patriarca, in: J.W. Davies, D.J. Michael (Eds.), Topical Conference on Ferritic Steels for Use in Nuclear Technologies, Metallurgical Society of AMIE, 1984, p. 107.
[7] J.E. Bynum, F.V. Ellis, B.W. Roberts, in: Symposium on Structural Materials for Service at Elevated Temperatures in Nuclear Power Generation, ASME, Houston, TX, 1975, p. 146.
[8] T.A. Parthasarathy, P.G. Shewmon, Metall. Trans. 15A (1984) 2021.
[9] T.A. Parthasarathy, P.G. Shewmon, Metall. Trans. 18A (1987) 1309.
[10] D. Stone, S. Ruoff, J. Wanagel, C.Y. Li, Fossil energy materials program, Quarterly report, ORNL/FMP/84/1/ 1984, p. 153.
[11] A.W. Thompson, I.M. Bernstein, in: M.G. Fontanna, R.W. Stahle (Eds.), The Role of Metallurgical Variables in Hydrogen Assisted Environment Fracture, Advances in Corrosion Science and Technology, Vol. 7, p. 53.
[12] R.D. Mc Cright, in: R.W.Stahle, J.Hochman, R.D. McCright, J.E.Slater (Eds.), Proceedings of the International Conference on Stress Corrosion Cracking and Hydrogen Embrittlement of Iron Base Alloys, Vol. 42, Unieux-Firminy, France, 1973, p. 306.
[13] T.P. Radhakrishnan, L.L. Shreir, Electrochim. Acta 12 (1967) 889.

[14] E. Snape, Corros.-NACE 24 (1968) 261.
[15] R.M. Hudson, G.L. Strgand, Corrosion 16 (1960) 253.
[16] S.L.I.Chan, H.L.Lee, J.R.Yang, in: N.D. Moody, A.W. Thompson (Eds.), Hydrogen Effects on Material Behaviour, The Mineral, Metals and Materials Society, 1990, p. 145.
[17] Y. Sakamoto, T. Mantani, Trans. JIM 17 (1976) 743.
[18] Y. Sakamoto, K. Takao, in: Proceedings of the Second International Congress on Hydrogen in Metals, Paris, France, 1977, paper 1A8, 6-11 VI (1977).
[19] K. Bolton, L.L. Shreir, Corros. Sci. 3 (1963) 17.
[20] C.D. Kim, A.W. Loginow, Corrosion 24 (1968) 313.
[21] W.W. Gerberich, in: I.M. Bernstein, A.W. Thompson (Eds.), Hydrogen in Metals, International Conference, September, 1973, Champion, PA, USA, ASM, 1974, p. 115.
[22] S. Saroja, M. Vijayalakshmi, V.S. Raghunathan, Mater. Trans. Jpn. Inst. Met. 34 (1993) 901.
[23] M. Vijayalakshmi, S. Saroja, V. Thomas Paul, R. Mythili, V.S. Raghunathan, Metall. Mater. Trans. A 30 (1999) 161.
[24] N. Parvathavarthini, S. Saroja, R.K. Dayal, J. Nucl. Mater. 264 (1999) 35.
[25] N. Parvathavarthini, R.K. Dayal, J.B. Gnanamoorthy, Corrosion 52 (1996) 540.
[26] M. Atkins (Ed.), Atlas of Continuous Cooling Transformation Diagrams for Engineering Steels, British Steel, Sheffield, England, 1982, p. 152.
[27] P. Parameswaran, M. Vijayalakshmi, P. Shankar, V.S. Raghunathan, J. Mater. Sci. 27 (1992) 5426.
[28] K. Kiuchi, R. McLellan, Acta Metall. 31 (1983) 961.
[29] R.A. Oriani, Acta Metall. 18 (1970) 147.
[30] J.P. Hirt, Metall. Trans. A 11A (1980) 861.
[31] T. Asaoka, in: Proceedings of the Second JIM International Symposium on Hydrogen in Metal, Minakami, Japan, 1979, p. 161.
[32] T. Asaoka, in: Nejat, Vezivoglu (Eds.), Proceedings of the Miami International Symposium on Metal Hydrogen System, 13–15 April, 1981, Miami beach, USA, Pergamon, p. 197.
[33] R. Valentini, A. Solina, Mater. Sci. Technol. 10 (1994) 908.
[34] Shaju K. Albert, PhD thesis, IIT, Mumbai, 1996.